

# An Ancient Massive Quiescent Galaxy Found in a Gas-rich $z \sim 3$ Group

Boris S. Kalita<sup>1</sup> , Emanuele Daddi<sup>1</sup> , Chiara D'Eugenio<sup>1</sup> , Francesco Valentino<sup>2,3</sup> , R. Michael Rich<sup>4</sup> , Carlos Gómez-Guijarro<sup>1</sup> , Rosemary T. Coogan<sup>5</sup> , Ivan Delvecchio<sup>6</sup> , David Elbaz<sup>1</sup> , James D. Neill<sup>7</sup> , Annagrazia Puglisi<sup>8</sup> , and Veronica Strazzullo<sup>6,9,10</sup> , Annagrazia Puglisi<sup>8</sup> , and Veronica Strazzullo<sup>6,9,10</sup> , Annagrazia Puglisi<sup>8</sup> , and Veronica Strazzullo<sup>6,9,10</sup> , James D. Neill<sup>7</sup> , Cea, Irfu, DAP, AIM, Universitè Paris-Saclay, Universitè de Paris, CNRS, F-91191 Gif-sur-Yvette, France; boris kalita@cea.fr 

<sup>2</sup> Cosmic Dawn Center (DAWN), Copenhagen, Denmark

<sup>3</sup> Niels Bohr Institute, University of Copenhagen, Jagtvej 128, DK-2200 Copenhagen, Denmark

<sup>4</sup> Department of Physics & Astronomy, University of California, Los Angeles, PAB 430 Portola Plaza, Los Angeles, CA 90095-1547, USA 

<sup>5</sup> Max-Planck-Institut für Extraterrestrische Physik (MPE), Giessenbachstr.1, D-85748 Garching, Germany 

<sup>6</sup> INAF-Osservatorio Astronomico di Brera, via Brera 28, I-20121, Milano, Italy

<sup>7</sup> California Institute of Technology, 1200 East California Boulevard, MC 278-17, Pasadena, CA 91125, USA 

<sup>8</sup> Centre for Extragalactic Astronomy, Department of Physics, Durham University, Durham, UK 

<sup>9</sup> University of Trieste, Piazzale Europa, 1, I-34127 Trieste TS, Italy 

<sup>10</sup> INAF-Osservatorio Astronomico di Trieste, via Tiepolo 11, I-34131 Trieste, Italy *Received 2021 June 1; revised 2021 July 13; accepted 2021 July 22; published 2021 August 16* 

#### Abstract

Deep Atacama Large Millimeter/submillimeter Array and Hubble Space Telescope observations reveal the presence of a quenched massive galaxy within the z=2.91 galaxy group RO-1001. With a mass-weighted stellar age of  $1.6\pm0.4$  Gyr this galaxy is one of the oldest known at  $z\sim3$ , implying that most of its  $10^{11}\,M_\odot$  of stars were rapidly formed at z>6-8. This is a unique example of the predominantly passive evolution of a galaxy over at least 3< z<6 following its high-redshift quenching and a smoking-gun event pointing to the early imprint of an age-environment relation. At the same time, being in a dense group environment with extensive cold gas reservoirs as betrayed by a giant Ly $\alpha$  halo, the existence of this galaxy demonstrates that gas accretion shutdown is not necessary for quenching and its maintenance.

Unified Astronomy Thesaurus concepts: High-redshift galaxies (734); Galaxy evolution (594); Galaxy groups (597)

#### 1. Introduction

Hydrodynamical simulations and semianalytical models have found it difficult to reproduce massive ( $\gtrsim 10^{11} M_{*}$ ) quiescent galaxies (QGs) beyond  $z \gtrsim 3$  (Steinhardt et al. 2016; Schreiber et al. 2018b; Cecchi et al. 2019), while observations have been pushing the redshift boundary by detecting such systems at  $z \sim 3$ –4 (Gobat et al. 2012; Glazebrook et al. 2017; Schreiber et al. 2018a; D'Eugenio et al. 2020a; Forrest et al. 2020a, 2020b; Saracco et al. 2020; Valentino et al. 2020). Most of the systems so far observed belong to a population of recently quenched "post-starburst" (PSB) galaxies with their last star formation episode occurring over the last <0.8 Gyr. However, we might still be missing a fraction of older ( $\gtrsim 1$  Gyr) QGs (D'Eugenio et al. 2020b; Forrest et al. 2020b). Moreover, there has not been any insight on the influence of the environment over such galaxies, as most of those studied are field objects.

Studying a younger subsample of a larger population of high-z QGs may have influenced our understanding of how quiescence occurs and persists. Currently, for star formation to be suppressed in the z>2 epoch that usually features gas-rich star-forming galaxies, there are a variety of possible channels. These include merger-driven starbursts (Puglisi et al. 2021), active galactic nucleus (AGN) feedback (Brennan et al. 2018), gas strangulation (Peng et al. 2015), halo quenching (Feldmann & Mayer 2015), and morphological quenching (Martig et al. 2009). Hence, further probing the high-z QG population, including those in dense environments, will provide opportunities to investigate the earliest mechanics of quenching.

With this in mind, we report the detection of an extremely red and old quiescent galaxy within a dense environment at  $z \sim 3$ . Throughout, we adopt a concordance  $\Lambda$ CDM cosmology,

characterized by  $\Omega_m = 0.3$ ,  $\Omega_{\Lambda} = 0.7$ , and  $H_0 = 70 \,\mathrm{km\,s}^{-1}$  Mpc<sup>-1</sup>. We use a Chabrier initial mass function. Magnitudes and colors are on the AB scale.

# 2. Galaxy-D and RO-1001

Three massive  $(\log(M_{\star}/M_{\odot}) \gtrsim 11)$  galaxies (A, B, and C in Figure 1; Daddi et al. 2021) in the z = 2.91 RO-1001 group have a combined star formation rate (SFR)  $\sim 1250 \, M_{\odot} \, \mathrm{yr}^{-1}$ . NOrthern Extended Millimeter Array (NOEMA) observations of the CO(3-2) transition showed that they lie at the same redshift of z = 2.91. Furthermore, the presence of extensive cold gas reservoirs is suggested by Ly $\alpha$  observations that revealed extended filaments converging onto a single massive halo with a combined luminosity of  $1.3 \pm 0.2 \times 10^{44}$  erg s<sup>-1</sup>, most likely still affected by cold accretion persisting in this system with an estimated dark matter halo mass of  $4 \times 10^{13} M_{\odot}$ . These conclusions are based on the observed line profile, the velocity field, and the energetics underlying the Ly $\alpha$  emission (Daddi et al. 2021). Moreover, also pointing to the availability of cold gas is the redshift of the group, which places it in the epoch where cold flow accretion is expected to dominate (Valentino et al. 2015; Overzier 2016). Galaxy-D was reported earlier as a possible passive member of RO-1001 (Figure 1; Daddi et al. 2021).

# 3. Observations

## 3.1. Optical and Near-IR Imaging

RO-1001 was observed with Hubble Space Telescope (HST)/WFC3 imaging in three bands (F160W, F125W, and F606W) over a total of 11 orbits during Cycle 27 (Proposal ID: 15190, PI: E. Daddi). The data reduction was executed using

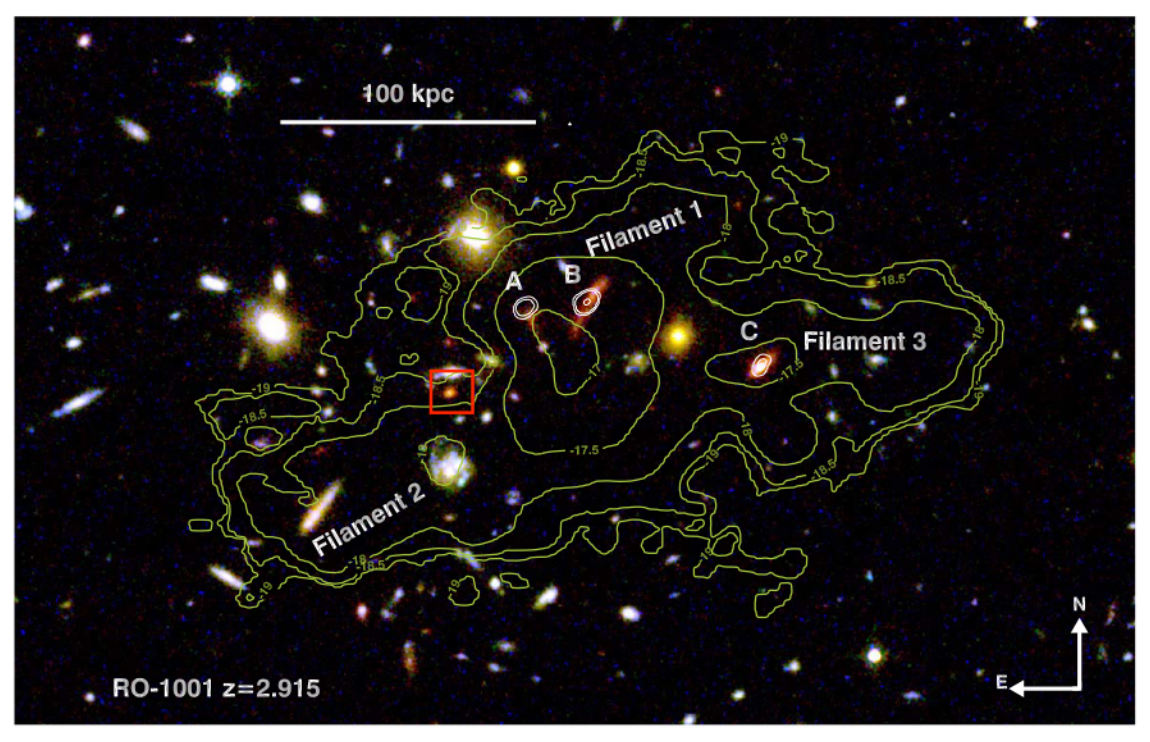


Figure 1. The core of RO-1001 as seen is HST/WFC3 (F606W, F125W, and F160W). The green contours denote the Ly $\alpha$  nebula luminosity with the locations of the associated filaments possibly powered by cold flow accretion (Daddi et al. 2021). Galaxy-D is marked with a red square.

the pipeline  $griz li.^{11}$  The  $5\sigma$  point-source sensitivities reached are 26.25 (F160W), 26.47 (F125W), and 26.39 (F606W) with a pixel scale of 0."06 and a half-power beamwidth of 0."24 for F160W. Public COSMOS F814W imaging was also incorporated into the analysis. Due to a lack of coverage in the z and y bands, we include Subaru Hyper Suprime-Cam images that were from the "COSMOS2015" database (Laigle et al. 2016). Furthermore, we used the Ks-band image from data release 4 of Ultra-VISTA. Finally, IRAC 3.6  $\mu$ m and 4.5  $\mu$ m images were taken from the Spitzer Matching Survey of the Ultra-VISTA Deep Stripes (SMUVS), while those at 5.8  $\mu$ m were taken from the COSMOS2015 database.

## 3.2. Submillimeter Imaging

To have an estimate of the obscured star formation down to very faint levels in RO-1001, and as a result on Galaxy-D, we also obtained submillimeter data. Atacama Large Millimeter/submillimeter Array (ALMA) band 7 observations were taken in Cycle 7 (Project ID: 2019.1.00399.S, PI: R. M. Rich). The data reduction was mainly carried out using the Common Astronomy Software Application (CASA). The final mosaics have a maximum sensitivity of  $28\,\mu\mathrm{Jy\,beam}^{-1}$ , with a synthesized beam size of 0."49 × 0."46.

## 4. Analysis and Results

# 4.1. Photometry

In the COSMOS2015 catalog (Laigle et al. 2016) Galaxy-D is blended with a galaxy located 1" to the north (Figure 1). Hence, we make new flux measurements for it in each of the wavelength windows we have access to. We first use SExtractor for the four HST/WFC3 images since the the resolution is sufficient to clearly

separate galaxy-D from its neighboring foreground galaxy. We use F160W as the detection image to carry out matched aperture photometry using isophotal radii. To ensure equivalent resolutions, we also convolve the F606W, F814W, and F125W images with Gaussians such that their respective final point-spread functions (PSFs) have the same size as that in F160W. From the catalog hence created, we find it to be undetected in F606W and F814W (which therefore provide upper limits), while F125W and F160W have clear detections with a signal-to-noise ratio (S/N) of  $\sim$ 25 and 65, respectively. The z and y bands also return nondetections, which are hence used to set flux upper limits.

In order to ensure that all of the flux from Galaxy-D is accounted for, we use galaxy morphological model fitting with the software GALFIT. Since the 1.6  $\mu$ m (F160W) image has the highest S/N, we use it for this attempt. We fit sérsic profiles to both Galaxy-D and the foreground galaxy, along with Gaussian profiles to multiple surrounding objects (Figure 2). We measure a total AB magnitude of 24.00 for Galaxy-D and get a Sérsic index of  $2.0 \pm 0.2$ . The error on the latter value includes the results from a coaddition of the F125W image to the F160W image to improve S/N as well as an independent analysis of the F125W image, all of which are in agreement. The Sérsic index suggests that this galaxy might feature a disky component with a significant bulge component, within the scatter expected from high-z QGs (Lustig et al. 2021). The galaxy is also found to be extremely compact with an effective radius,  $r_e = 0.14 \pm 0.103$ , which at z = 2.9 is  $1.1 \pm 0.1$  kpc. We further use the flux difference between the GALFIT measurement and that from SExtractor, to scale up the catalog (isophotal) flux measurement at 1.25 µm (F125W) as well as the upper limits at 0.6  $\mu$ m (F606W) and 0.8  $\mu$ m (F814W).

The morphological properties of Galaxy-D determined through the model fitting at  $1.6 \,\mu m$  are further used as priors in the Ks band (2.1  $\mu m$ ) as well as IRAC 3.6, 4.5, and 5.8  $\mu m$ . This is done in order to deblend the galaxy from its foreground neighbors, which are also simultaneously fit with models based

<sup>11</sup> https://github.com/gbrammer/grizli

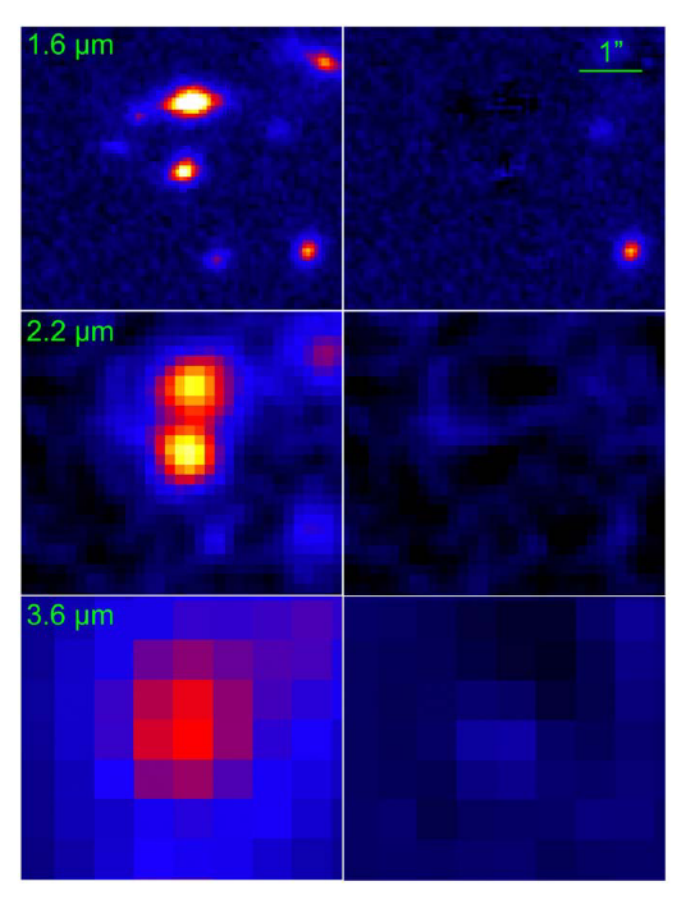


Figure 2. Panels showing Galaxy-D (at the center) along with its surrounding foreground galaxies in three out of the five wavelength bands for which GALFIT was used to extract the photometry. As detailed in Section 4.1, the results of the H band (1.6  $\mu$ m) were used to deblend at the other bands (2.2  $\mu$ m, 3.6  $\mu$ m, 4.5  $\mu$ m, and 5.8  $\mu$ m, the first two of which are shown in the middle and lower rows, respectively). More sources were fit and subtracted at longer wavelengths due to the increase in PSF size. The residual images are found to not have any fluctuations >1 $\sigma$ .

on 1.6  $\mu$ m priors (Figure 2). Images beyond this wavelength window do not show a detection, while the implied upper limits are not constraining, and are hence not used.

# 4.2. SED Fitting

We fit the photometry derived in the previous section with BC03 stellar population models (Bruzual & Charlot 2003) to derive the properties of Galaxy-D (Figure 3, top left). We use HYPERZ to determine the best-fitting spectral energy distribution (SED) templates through a  $\chi^2$  minimization procedure. We investigate a redshift range of 0–6 with a step size of 0.01. For the BC03 templates, a range of metallicities are allowed ( $\frac{1}{5}Z_{\odot}$ ,  $\frac{1}{2}Z_{\odot}$ ,  $Z_{\odot}$ , and  $\frac{5}{2}Z_{\odot}$ ). We also implement the Calzetti et al. (2000) law along with Small and Large Magellanic Cloud laws for dust attenuation, with extinction values,  $A_{\rm V}=0$ –7, in steps of 0.025. Finally, a wide variety of star formation histories (SFHs) are used:

- 1. Simple stellar population (SSP): This is the most basic model with all of the stellar mass formed during an infinitesimal short burst of star formation at t = 0.
- 2. Constant star formation models: Although we have enough evidence for the quiescence of the galaxy (discussed in

- detail in Section 5.1), we use this model featuring no decline in star formation (it remains constant throughout) to check if a high attenuation star-forming scenario is formally consistent with the available photometry.
- 3. Truncated models: These involve a constant SFR from t=0 up until a  $t_{\text{stop}}$ , beyond which SFR =  $0\,M_{\odot}\,\text{yr}^{-1}$ . The  $t_{\text{stop}}$  is varied from 0.1 Gyr to a generous upper limit of 5.0 Gyr in steps of 0.1 dex.
- 4. Delayed  $\tau$ -models: Finally, we use an SFH that has been widely preferred to model QGs. The exponentially declining SFH here is characterized as  $\propto (t/\tau^2)e^{-t/\tau}$  with a peak of star formation at  $t = \tau$ . The  $\tau$  varies within [0.1, 5.0] Gyr with steps of 0.05 dex.

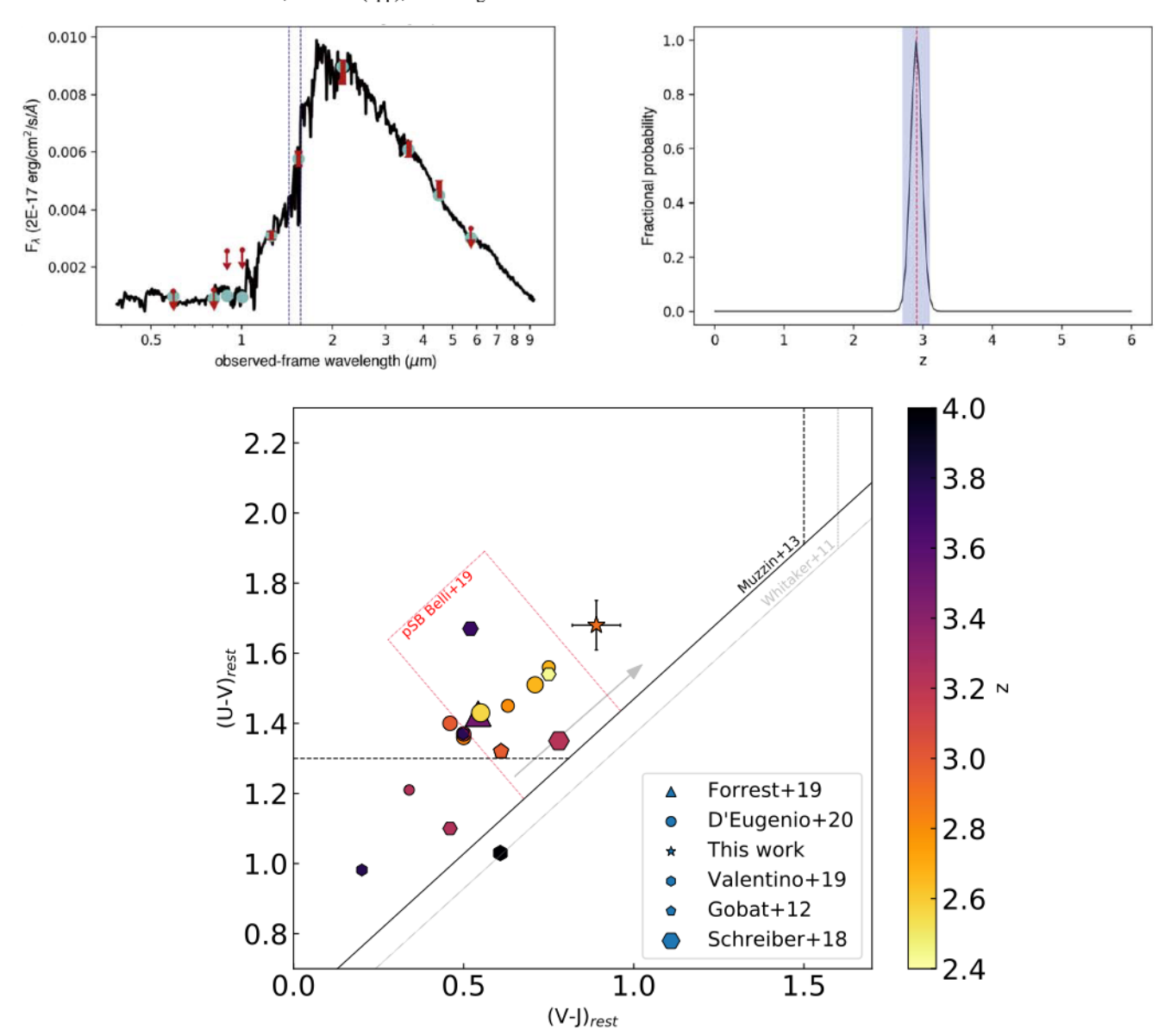
We investigate the reduced  $\chi^2$  values from the fits using the various BC03 models, over the above-mentioned grid of  $A_{\rm V}$ . We get the best fit with the delayed  $\tau$ -models (with a reduced  $\chi^2 \sim 0.4$ ), closely followed by SSP and truncated models. In comparison, we find a complete lack of fit using the constant star formation templates ( $\Delta \chi^2 > 30$ ), with any level of reddening, reinforcing our claim of Galaxy-D being quiescent.

#### 4.3. Galaxy Parameters

The photometric redshift (photo-z) determined from the SED fitting is found to be  $2.9 \pm 0.1$  (Figure 3, top right), with the limits giving the  $1\sigma$  confidence interval ( $\Delta\chi^2 < 1$ ). We also derive a stellar mass,  $\log(M_*/M_\odot) = 11.0 \pm 0.2$ , in agreement with the previous results in Daddi et al. (2021). Moreover, we find minimum levels of attenuation with the fitting procedure returning a value of  $A_V \sim 0.1$ . We further confirm that our choice of gridding and "edge-effects" do not influence our results by investigating a variety of grids for  $A_V$  while ensuring that the parameter space on both sides of the best-fit value is well sampled.

Following the analysis in similar studies (Gobat et al. 2012; Schreiber et al. 2018b; D'Eugenio et al. 2020a; Valentino et al. 2020), we define  $t_{50}$ , which is the time elapsed since the epoch of "half-mass formation" up until the time of observation. We determine this quantity to be  $1.6 \pm 0.4$  Gyr at 90% confidence, after marginalizing on all the unknown parameters (SFH, metallicity, dust attenuation law and  $A_V$ , and redshift). Fixing metallicity to solar does not change our results. Studying each of the values, we find that  $t_{50}$  gets progressively lower as we go from subsolar to supersolar metallicities. At z = 2.9, for  $\frac{1}{5}Z_{\odot}$ , we derive a best-fit  $t_{50} \sim 2.2$  Gyr that is almost equal to the age of the universe at that redshift, while for the supersolar  $\frac{3}{2}Z_{\odot}$ , the  $t_{50}$  is found to be  $\sim 1.0$  Gyr. Although these results incorporate all previously mentioned SFH models together, using each model separately we find that the results from delayed- $\tau$  and truncated models are in agreement, while those using SSP (which can be considered as the light-weighted age) push the age upper limit by  $\sim 0.2$  Gyr. Finally, fixing the redshift to that of RO-1001 (z = 2.91) does not change the constraint on the age estimate.

We also investigate the robustness of our measurements with simulations. We perturb the flux measurements with values drawn within Gaussians with sigma equal to the  $1\sigma$  uncertainty of the respective flux measurement to generate 1000 sets of photometric data points. Besides a consistent average best-fit age of 1.7 Gyr, we find the  $1\sigma$  scatter to be 0.15 Gyr (once accounting for the gridding effect). This uncertainty is slightly lower than the 0.2 Gyr ( $1\sigma$  or 68% confidence interval;



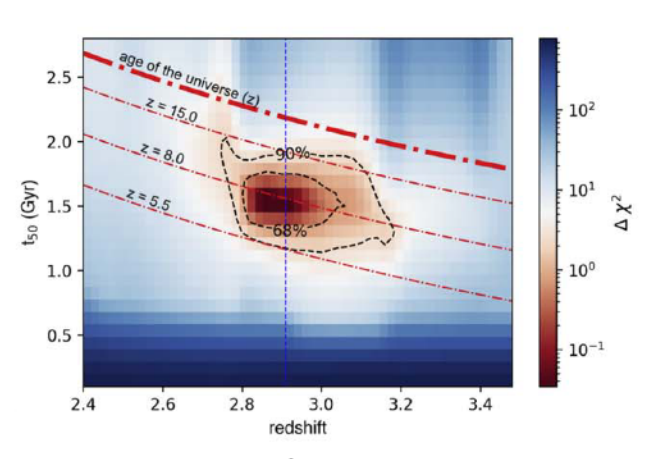
**Figure 3.** (Top left) The best-fit SED template using the available photometry for Galaxy-D. The red bars show the observed photometry while the cyan points mark the expected values from the SED. The blue dashed lines mark the locations of the Balmer and 4000 Å breaks. (Top right) The probability distribution function for the photometric redshift of Galaxy-D. The red dashed line marks the spectroscopic redshift of RO-1001, while the blue shaded region marks the 90% confidence region of the photometric redshift for Galaxy-D. (Bottom) The UVJ colors of high-z QGs (z > 2.5) adapted from D'Eugenio et al. (2020a). The gray arrow shows the expected color evolution with increasing age. Galaxy-D is marked with a star, clearly outside the PSB region specified in Belli et al. (2019). The marker sizes are proportional to the stellar mass.

Figure 4, left) that we get from the  $\Delta$   $\chi^2$  analysis. We repeated the exercise perturbing the best-fit SED photometry instead of the observed photometry, finding the same results. Furthermore, for both cases, we also check the possible consequences of asymmetry in the range of acceptable ages in each fit ( $\Delta$   $\chi^2$  < 1) by taking an average of their values. This also returns an age of 1.7 Gyr. Hence, we do not revise our more conservative results from the latter technique quoted throughout this work.

Furthermore, in order to have an SFH model-independent assessment of Galaxy-D within the framework of QGs at high-z, we also plot the  $(UVJ)_{\rm rest}$  colors (Figure 3, bottom). These are determined using the F160W, Ks, and IRAC 4.5  $\mu$ m photometry, that match nearly perfectly to the rest-frame U, V, and J bands, with small correction for the residual differences in effective wavelengths adopted from the best-fitting SED.

#### 4.4. Uniqueness and RO-1001 Membership

The photo-z measurement of  $2.9\pm0.1$ , which is in remarkable agreement with the  $z_{\rm spec}=2.91$  of RO-1001, strongly suggests group membership. This is further reinforced by the vanishingly low probability of  $\sim 3\times 10^{-5}$  for a chance alignment of Galaxy-D within 10" from the center of the RO-1001 group (as defined by the peak of the Ly $\alpha$  emission). This is estimated by the implied surface density of the 20 galaxies with H-band magnitudes  $\leq 24.0$ , J-H color  $\geq 1.1$ , and H-Ks color  $\geq 2.2$  over the whole COSMOS area (Laigle et al. 2016). The color-selection thresholds determined by the photometry of Galaxy-D also incorporate the uncertainties in the measurements. However, 16/20 of these galaxies are consistent with being selected due to the  $1\sigma$  scatter in their color measurements (recall that the COSMOS catalog contains more than half



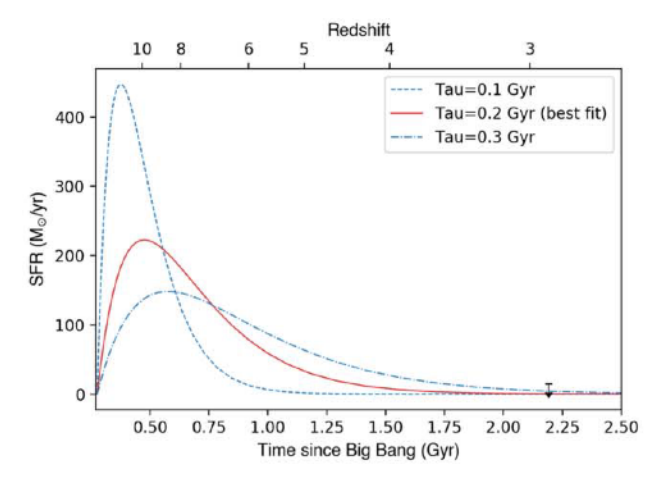


Figure 4. (Left) The variation of  $\Delta \chi^2$  in the stellar population age  $(t_{50})$  vs. redshift space. The dotted–dashed lines demarcate the lookback times for various redshifts along with the thickest of them showing the age of the universe, all of which are functions of redshift. (Right) The best-fit delayed  $\tau$ -model SFH ( $\tau = 0.2$  Gyr) as a function of age of the universe as well as redshift. Also shown are the SFH models with  $\tau = 0.1$ , 0.3 Gyr, which are within the 90% confidence interval. Finally, the SFR  $2\sigma$  upper limit of  $13~M_{\odot}$  yr $^{-1}$  derived from the ALMA 870  $\mu$ m nondetection is shown with the black downward arrow.

million sources). Hence, this number of objects found can be considered as a generous upper limit. The lack of deep HST data like those we have for Galaxy-D primarily influences this conclusion. Out of the remaining 4/20, two lack photometry in most of the COSMOS observation bands and therefore do not have a photo-z reported in the catalog. The final two galaxies (Laigle IDs: 749600 and 824982<sup>12</sup>) are the only objects in the 2 deg<sup>2</sup> area of COSMOS, which have been robustly found to have similar observed characteristics within the framework of the state-of-the-art multiwavelength database available for the field. Also as a consequence, these galaxies have similar redshift, mass, and age estimates as for Galaxy-D. However, due to a lack of submillimeter data (and therefore a confirmation of quiescence) along with any environmental information, a thorough study for these objects cannot be currently undertaken. However, this lack of counterparts should not be regarded as a suggestion of similar objects being absent. Rather, this could simply point to the inefficiency of current surveys to detect such galaxies with a high completeness, making Galaxy-D extremely rare within the current detection limits of surveys.

Hence, besides being very unique, it is extremely unlikely that this galaxy is at a redshift different from that of the group RO-1001. Although, it cannot be currently determined with certainty whether Galaxy-D is exactly within the core of RO-1001 or part of the associated large-scale structure. In either case Galaxy-D can still be considered to be within a dense environment.

#### 5. Discussion

# 5.1. Quiescence and the Last Epoch of Star Formation

Confirmation of quiescence at such high redshifts can be challenging (Glazebrook et al. 2017; Schreiber et al. 2017; Simpson et al. 2017). However for Galaxy-D, the optical and NIR colors suggest a lack of star formation based on a complete disagreement with the star-forming SFH models (Section 4.2). Taking into account all possible SFH models (within 90% confidence interval), we determine an SFR upper limit of  $4 \, M_{\odot} \, \text{yr}^{-1}$ , ×30 below the main sequence (MS).

The nondetection in our deep ALMA 870  $\mu$ m data (Section 3.2) is used to determine a  $2\sigma$  upper-limit SFR (conservative; fully accounting for its spatial extent of NIR emission of the galaxy based on its Sérsic profile) of  $13\,M_\odot$  yr<sup>-1</sup> assuming conservatively a main-sequence template appropriate for z=3 (Béthermin et al. 2012). This is already a factor  $\sim$ 10 below the main sequence at  $z\sim3$  (Santini et al. 2017). The limit would be a further factor of 2 deeper if assuming instead a colder IR SED following Gobat et al. (2018), i.e., at  $\times$ 20 below the MS. Hence, it can be unambiguously concluded that Galaxy-D is truly quiescent, consistently from both the optical and IR sides.

Based on the mass-weighted ( $t_{50}$ ) as well as light-weighted age limits (Section 4.3), the primary episode of star formation had already elapsed by  $z \gtrsim 6$  and most likely by  $z \sim 8$  (Figure 4, left), right after which it likely experienced a rapid decline in its SFR characterized by the best-fit delayed  $\tau$ -model with  $\tau = 0.2$  Gyr (Figure 4, right). However, this should be considered as an approximate upper limit, since  $\tau = 0.1$  Gyr and the SSP (which has  $\tau$  equivalent to 0) also return acceptable fits (within an overall  $\Delta \chi^2 < 1$  or 68% confidence interval).

This form of rapid quenching has been extensively proposed to explain populations of QGs at  $z \sim 3-4$  (e.g., Schreiber et al. 2018b; D'Eugenio et al. 2020a, 2020b; Forrest et al. 2020a, 2020b; Valentino et al. 2020). However, these are usually found to be PSBs, with  $t_{50} < 0.8$  Gyr (Figure 5). Such studies usually leave out galaxies similar to Galaxy-D that are expected to have an older (>1 Gyr) stellar population, due to preferential selection of brighter targets. Forrest et al. (2020b) show that galaxies with such ages would be considerably less bright (by  $\sim$ 1–2 mag) in near-IR (NIR), compared to PSBs. For example, in comparison to Galaxy-D, the Valentino et al. (2020) and D'Eugenio et al. (2020b) samples in the Ks band are on average brighter by 1.7 and 2.4 mag, respectively. This is also the case for a very recent detection of a ~0.6 Gyr old massive OG detected in a protocluster environment at z = 3.1, with a Ksband magnitude 1.3 brighter (Kubo et al. 2021). This difference is also found to manifest in the SFH-independent UVJ diagram (Figure 3, bottom), which clearly shows a marked separation in color and hence an inferred age between the well-studied PSB population and Galaxy-D.

<sup>&</sup>lt;sup>12</sup> R.A., decl.: (149.47703, 2.43692) and (149.52635, 2.55155).

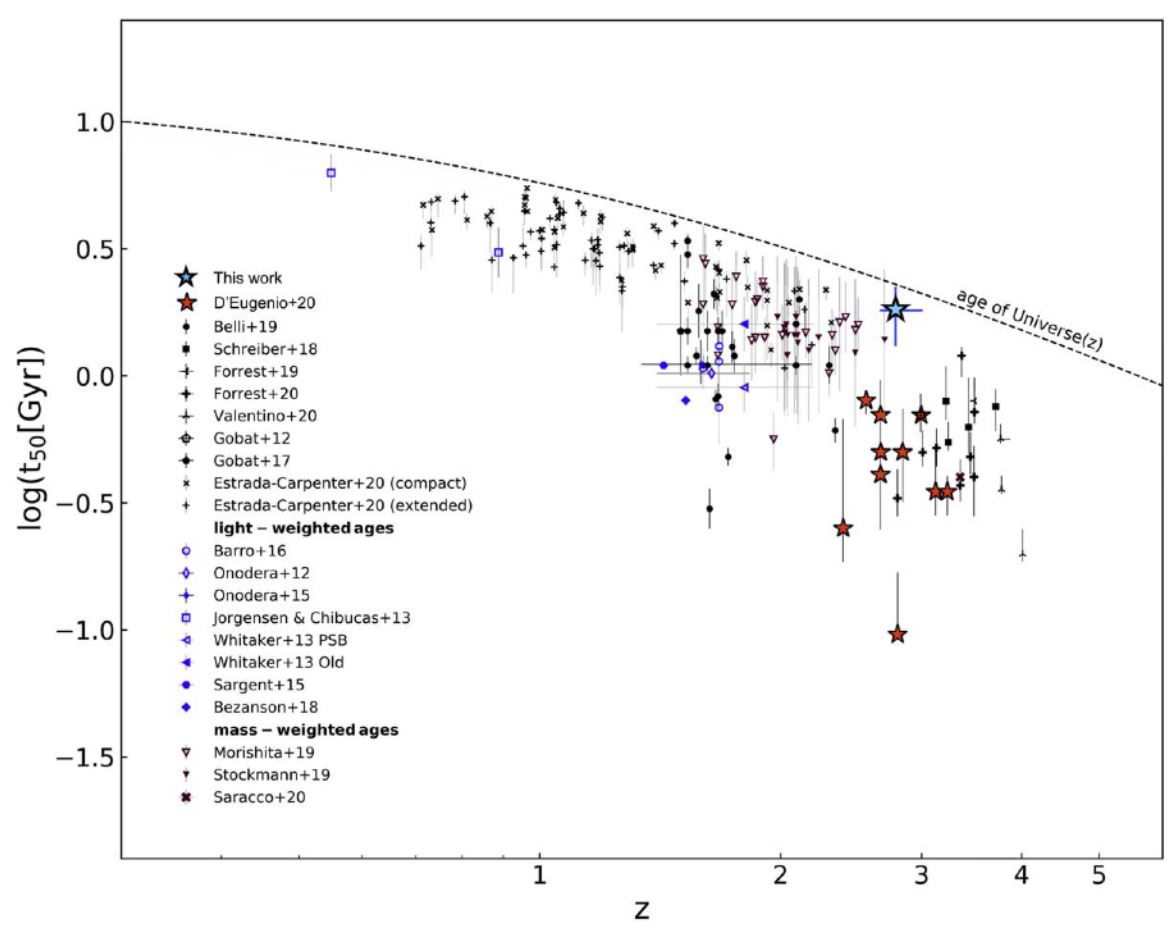


Figure 5. The stellar population age  $(t_{50})$  vs. redshift distribution for  $\log(M_*/M_\odot) > 10.5$  QGs adapted from D'Eugenio et al. (2020b), with the references therein. Although the definition of the "mass-weighted ages" for a subset of the works add a level of ambiguity, they are found to be in agreement with our definition of  $t_{50}$  within a maximum of 0.1 Gyr (although in the case of Morishita et al. 2019, their "mass-weighted age" is equal to  $t_{50}$ ). We add Galaxy-D (light-blue star) with the 90% confidence intervals shown as the error bars for both axes.

Hence, spectroscopic analysis of such very old galaxies is much more difficult, with requirements of extremely long integration times. Possibly as a result, similarly old galaxies at  $z \sim 3$  have not yet been spectroscopically studied yet (Figure 5). We do acknowledge the presence of a population of galaxies at  $z \sim 2-2.7$  in Figure 5 with seemingly similar ages from Morishita et al. (2019). But this comparison is affected by systematics, as their age estimates from bursty star formation histories would be lowered by a factor of  $\sim 1.5-2.0$  if smooth SFH models are employed as in our study (see Figure 12 in Morishita et al. 2019), further emphasizing the unicity of Galaxy-D in the panorama of known old galaxies at  $z \sim 3$ .

Larger photometric studies, also with higher uncertainties regarding galaxies being truly quiescent, primarily feature young stellar populations with an extremely small fraction of their samples having ages >1 Gyr (e.g., Straatman et al. 2014; Carnall et al. 2020). We do have examples of galaxies at lower redshifts  $z \sim 0.5$ –2 with old enough stellar populations suggesting that they should be already >1 Gyr old at z > 3 (Tacchella et al. 2021, and references therein). If those age inferences are correct (it is increasingly difficult at lower z to accurately project star formation histories at the earliest times), it is still possible that the progenitors of the lower-z oldest galaxies were not yet hierarchically assembled into a single galaxy by  $z \sim 3$  (Mancini et al. 2019). It is hence unclear whether old massive galaxies at  $z \sim 3$  are rare due to them

experiencing reaccretion of gas and returning back to a starforming population, to not having yet assembled, or they have simply not yet been detected at these redshifts. Future timeintensive studies would hence be required to complete the mapping of high-z QGs in this regime. A crucial diagnostic for such attempts would be the Balmer and 4000 Å breaks characterized by  $D_B$  (Kriek et al. 2006) and  $D_n$ 4000 (Balogh et al. 1999), respectively. The transition of the  $D_B/D_n4000$ ratio toward values <1 is a tell-tale sign of ages  $\gtrsim 1.0 \,\mathrm{Gyr}$ (D'Eugenio et al. 2020b). As an example, we calculate  $D_B/D_n4000 = 0.94$  from the best-fit SED template (Figure 3, top left), suggesting a small value for  $D_B$ . This is in stark contrast to the PSB population, which is usually characterized by much stronger Balmer breaks and hence higher  $D_B/D_n4000$ ratios (e.g., D'Eugenio et al. 2020b find an average value of 1.53 for their sample). Future spectroscopy, that should be within reach of the James Webb Space Telescope, will be needed to validate these inferences.

## 5.2. Tracing the Evolution

The short characteristic timescales (Figure 4) and compact nature of Galaxy-D ( $r_e = 1.1 \pm 0.1$  kpc at z = 2.9) can be explained by scenarios like mergers (e.g., Puglisi et al. 2021) that drive gas into a compact central region of the galaxy, leading to rapid consumption of gas through star formation. This quickly exhausts the available gas, thereby quenching the

system and leaving behind a compact QG. Compact star-forming cores possibly related to mergers are already observed in the three primary star-forming galaxies in RO-1001 that are nearly identical in mass and size to Galaxy-D (Daddi et al. 2021; B. S. Kalita et al. 2021, in preparation), but forming stars at a rate of over  $1000 \, M_{\odot}$  yr  $^{-1}$  in total.

Furthermore, with 50% stellar mass ( $\sim 5 \times 10^{10} M_{\odot}$ ) being formed at  $z \ge 6$ , we can determine whether its progenitor could have existed based on the expected galaxy mass function, mainly sensitive to star-forming galaxies, at such redshifts. To make a comparison, we estimate a log number density of  $-7.2 \pm 0.5$  Mpc<sup>3</sup> by assuming a single detection within 2.6 < z < 3.2 over the COSMOS  $1.7^{\circ} \times 1.7^{\circ}$  area. Then a number density of  $>5 \times 10^{10} M_{\odot}$  possible progenitors at z > 5.5 is derived from the results of Grazian et al. (2015). We find the Galaxy-D-based density to be almost an order of magnitude lower than the latter value determined from the galaxy mass function. Including the two candidate "ancient" QGs discussed in Section 4.4 brings this down to a factor  $\sim$ 3, with the possibility of a further decrease if a few of the rest are found to also have similar properties. Nevertheless, it cannot yet be ascertained whether more galaxies with formation epochs at  $z \gtrsim 6$  within the COSMOS field do actually exist at similar redshifts. We can conclude, however, that at least 10% of the z > 6 star-forming galaxies with stellar mass  $>5 \times 10^{10} M_{\odot}$  can be expected to have undergone quenching by  $z \sim 6$  to form old QGs like Galaxy-D by  $z \sim 3$ .

#### 5.3. Quiescence in a Dense Environment

Given the estimated  $t_{50}$ , not only do we need a quenching mechanism that could form it very early, but any galaxy rejuvenation has to be prevented thereafter. This primarily involves curbing accretion of gas or preventing the gas from forming stars. Galaxy-D belongs to RO-1001 or associated subhalos at z = 2.91 (Section 4.4). This halo is expected to be fed by copious cold gas accretion (Daddi et al. 2021) still at z = 2.91, all the more in its past evolutionary and assembly phases and up to the z > 6 quenching of Galaxy-D that inescapably happened in a progenitor halo in which accretion must have been prominent. This shows that one may have quenching and keep fully quenched galaxies (that remain so for over 1 Gyr at z > 3-6) even with large amounts of diffuse cold gas and in presence of cold accretion. This is evidence that environmental quenching scenarios like cosmological starvation (Feldmann & Mayer 2015) and gas strangulation (Peng et al. 2015) do not play a necessary role in quenching and/or maintaining the quiescence of high-z galaxies.

One of the alternative channels for inhibiting star formation would be AGN-driven feedback (Sanders et al. 1988; Di Matteo et al. 2005; Hopkins et al. 2006; McCarthy et al. 2011). Although Galaxy-D is not hosting a detectable AGN (Daddi et al. 2021), multiple works have suggested that there are enhanced AGN fractions in high-z massive QGs (e.g., Olsen et al. 2013; Aird et al. 2019). Hence, it is highly likely that this galaxy would have at least experienced episodes of AGN activity in the past, inevitable given its large stellar mass. These AGN episodes might have or not curbed star formation as in QSO-mode quenching. However, AGN radio-mode activity was most likely crucial to allow it to evolve passively for >1 Gyr, as supported by the high radio detection rate of distant quenched systems (Gobat et al. 2018; D'Eugenio et al. 2020b). Furthermore, other scenarios like morphological quenching (stellar bulges preventing the collapse

of gas for star formation; Martig et al. 2009) could also be at play to prevent any significant late-time star formation.

But a question still remains: what sets Galaxy-D apart from the other similarly massive but intensively star-forming galaxies in RO-1001? It appears to be simply at a later evolutionary phase, while its vigorously star-forming counterparts have grown their large stellar masses later and are still undergoing rapid growth. They might have an eventual fate as that of Galaxy-D (similar to the scenario outlined in Puglisi et al. 2021), and be hardly distinguishable in the stellar population properties once reaching  $z \sim 0$  more than 10 Gyr later. While Galaxy-D has a massweighted age ( $t_{50}$ ) of 1.6  $\pm$  0.4 Gyr, most other quiescent galaxies at similar redshifts or above are younger PSBs and can predominantly be characterized as field galaxies (due to a lack of association with known overdensities). Therefore, the age difference between Galaxy-D and the currently known PSB population  $\sim 1.0$  Gyr is one of the first known evidence of an ageenvironment relation at high z. Interestingly, a similar difference of 1 Gyr between clusters and field has also been found for local populations, where this relation has already been established (e.g., Bernardi et al. 2006; Gallazzi et al. 2021). Similar, but relatively tentative trends have also been detected at  $z \sim 1.0-1.5$  (Webb et al. 2020). But unlike at low z, the age offset at  $z \gtrsim 3$  is a sizable fraction of the stellar ages themselves, thereby manifesting as much more pronounced observational differences as has already been discussed in Section 5.1.

In any case, Galaxy-D satisfying such a relation suggests a rapid hierarchical buildup of mass in dense environments, earlier than in the field. This in turn leads to the quenching scenarios discussed in the previous sections, mostly driven by mass and internal processes, while still agreeing with our conclusions of direct environment-dependent quenching scenarios not being necessary.

We would like to express our gratitude to Raphael Gobat for his valuable inputs. We also thank Gabriel Brammer for assistance with the use of grizli for the HST data reduction. R.M.R. and J.D.N. acknowledge support from GO15910. V.S. acknowledges the support from the ERC-StG ClustersXCosmo grant agreement 716762. F.V. acknowledges support from the Carlsberg Foundation Research Grant CF18-0388 "Galaxies: Rise and Death" and from the Cosmic Dawn Center of Excellence funded by the Danish National Research Foundation under then grant No. 140. A.P. gratefully acknowledges financial support from STFC through grants ST/T000244/1 and ST/P000541/1. B.S.K. would like to thank William G. Hartley (ETH Zurich, Switzerland), for providing crucial software-related files that were needed for this work. This paper makes use of the following ALMA data: 2019.1.00399. ALMA is a partnership of ESO (representing its member states), NSF (USA) and NINS (Japan), together with NRC (Canada), MOST and ASIAA (Taiwan), and KASI (Republic of Korea), in cooperation with the Republic of Chile. The Joint ALMA Observatory is operated by ESO, AUI/NRAO and NAOJ.

Software: SExtractor (Bertin & Arnouts 1996), GALFIT (Peng et al. 2002, 2010), grizli (v0.4.0; Brammer 2018), CASA (McMullin et al. 2007), HYPERZ (Bolzonella et al. 2000).

#### **ORCID iDs**

Boris S. Kalita https://orcid.org/0000-0001-9215-7053 Emanuele Daddi https://orcid.org/0000-0002-3331-9590 Chiara D'Eugenio https://orcid.org/0000-0001-7344-3126

```
Francesco Valentino https://orcid.org/0000-0001-6477-4011

R. Michael Rich https://orcid.org/0000-0003-0427-8387

Carlos Gómez-Guijarro https://orcid.org/0000-0002-4085-9165

Rosemary T. Coogan https://orcid.org/0000-0002-4343-0479

Ivan Delvecchio https://orcid.org/0000-0001-8706-2252

David Elbaz https://orcid.org/0000-0002-7631-647X

James D. Neill https://orcid.org/0000-0002-0466-1119

Annagrazia Puglisi https://orcid.org/0000-0001-9369-1805

Veronica Strazzullo https://orcid.org/0000-0001-7975-2894
```

#### References

```
Aird, J., Coil, A. L., & Georgakakis, A. 2019, MNRAS, 484, 4360
Balogh, M. L., Morris, S. L., Yee, H. K. C., et al. 1999, ApJ, 527, 54
Belli, S., Newman, A. B., & Ellis, R. S. 2019, ApJ, 874, 17
Bernardi, M., Nichol, R. C., Sheth, R. K., et al. 2006, AJ, 131, 1288
Bertin, E., & Arnouts, S. 1996, A&AS, 117, 393
Béthermin, M., Daddi, E., Magdis, G., et al. 2012, ApJL, 757, L23
Bolzonella, M., Miralles, J.-M., & Pelló, R. 2000, A&A, 363, 476
Brammer, G. 2018, gbrammer/grizli: Preliminary Release, Zenodo, doi:10.
   5281/zenodo.1146905
Brennan, R., Choi, E., Somerville, R. S., et al. 2018, ApJ, 860, 14
Bruzual, G., & Charlot, S. 2003, MNRAS, 344, 1000
Calzetti, D., Armus, L., Bohlin, R. C., et al. 2000, ApJ, 533, 682
Carnall, A. C., Walker, S., McLure, R. J., et al. 2020, MNRAS, 496, 695
Cecchi, R., Bolzonella, M., Cimatti, A., et al. 2019, ApJL, 880, L14
Daddi, E., Valentino, F., Rich, R. M., et al. 2021, A&A, 649, A78
D'Eugenio, C., Daddi, E., Gobat, R., et al. 2020a, ApJL, 892, L2
D'Eugenio, C., Daddi, E., Gobat, R., et al. 2020b, arXiv:2012.02767
Di Matteo, T., Springel, V., & Hernquist, L. 2005, Natur, 433, 604
Feldmann, R., & Mayer, L. 2015, MNRAS, 446, 1939
Forrest, B., Annunziatella, M., Wilson, G., et al. 2020a, ApJL, 890, L1
```

```
Forrest, B., Marsan, Z. C., Annunziatella, M., et al. 2020b, ApJ, 903, 47
Gallazzi, A. R., Pasquali, A., Zibetti, S., et al. 2021, MNRAS, 502, 4457
Glazebrook, K., Schreiber, C., Labbé, I., et al. 2017, Natur, 544, 71
Gobat, R., Daddi, E., Magdis, G., et al. 2018, NatAs, 2, 239
Gobat, R., Strazzullo, V., Daddi, E., et al. 2012, ApJL, 759, L44
Grazian, A., Fontana, A., Santini, P., et al. 2015, A&A, 575, A96
Hopkins, P. F., Hernquist, L., Cox, T. J., et al. 2006, ApJS, 163, 1
Kriek, M., van Dokkum, P. G., Franx, M., et al. 2006, ApJ, 645, 44
Kubo, M., Umehata, H., Matsuda, Y., et al. 2021, arXiv:2106.10798
Laigle, C., McCracken, H. J., Ilbert, O., et al. 2016, ApJS, 224, 24
Lustig, P., Strazzullo, V., D'Eugenio, C., et al. 2021, MNRAS, 501, 2659
Mancini, C., Daddi, E., Juneau, S., et al. 2019, MNRAS, 489, 1265
Martig, M., Bournaud, F., Teyssier, R., et al. 2009, ApJ, 707, 250
McCarthy, I. G., Schaye, J., Bower, R. G., et al. 2011, MNRAS, 412, 1965
McMullin, J. P., Waters, B., Schiebel, D., Young, W., & Golap, K. 2007, in
   ASP Conf. Ser. 376, Astronomical Data Analysis Software and Systems
   XVI, ed. R. A. Shaw, F. Hill, & D. J. Bell (San Francisco, CA: ASP), 127
Morishita, T., Abramson, L. E., Treu, T., et al. 2019, ApJ, 877, 141
Olsen, K. P., Rasmussen, J., Toft, S., et al. 2013, ApJ, 764, 4
Overzier, R. A. 2016, A&ARv, 24, 14
Peng, C. Y., Ho, L. C., Impey, C. D., & Rix, H.-W. 2002, AJ, 124, 266
Peng, C. Y., Ho, L. C., Impey, C. D., & Rix, H.-W. 2010, AJ, 139, 2097
Peng, Y., Maiolino, R., & Cochrane, R. 2015, Natur, 521, 192
Puglisi, A., Daddi, E., Brusa, M., et al. 2021, NatAs, 5, 319
Sanders, D. B., Soifer, B. T., Elias, J. H., et al. 1988, ApJ, 325, 74
Santini, P., Fontana, A., Castellano, M., et al. 2017, ApJ, 847, 76
Saracco, P., Marchesini, D., La Barbera, F., et al. 2020, ApJ, 905, 40
Schreiber, C., Elbaz, D., Pannella, M., et al. 2018a, A&A, 609, A30
Schreiber, C., Glazebrook, K., Nanayakkara, T., et al. 2018b, A&A, 618,
  A85
Schreiber, C., Pannella, M., Leiton, R., et al. 2017, A&A, 599, A134
Simpson, J. M., Smail, I., Wang, W.-H., et al. 2017, ApJL, 844, L10
Steinhardt, C. L., Capak, P., Masters, D., et al. 2016, ApJ, 824, 21
Straatman, C. M. S., Labbé, I., Spitler, L. R., et al. 2014, ApJL, 783, L14
Tacchella, S., Conroy, C., Faber, S., et al. 2021, arXiv:2102.12494
Valentino, F., Daddi, E., Strazzullo, V., et al. 2015, ApJ, 801, 132
Valentino, F., Tanaka, M., Davidzon, I., et al. 2020, ApJ, 889, 93
Webb, K., Balogh, M. L., Leja, J., et al. 2020, MNRAS, 498, 5317
```